Application of Two-Dimensional Orthogonal Wavelets to Multiresolution Image Analysis of a Turbulent Jet*[1]

By Hui Li,*[2] Masahiro Takei,*[3] Mitsuaki Ochi,*[3]
Yoshifuru Saito*[4] and Kiyoshi Horii*[5]

Key Words: Coherent Structure, Jet, Two-Dimensional Orthogonal Wavelet Transform, Turbulence, Vortex

Abstract

This paper develops an application of two-dimensional orthogonal wavelets to turbulence for the identification of multiresolution turbulent structures and coherent structures. The digital imaging slice photographs of a turbulent jet in a far field with $Re \cong 4.5 \times 10^3$ and 9.0×10^3 are respectively decomposed into six image components with different broader scales by wavelet multiresolution analysis. These image components provide visualized information on the multi-scale structures in a turbulent jet. It was found that the edges of the vortices at different resolutions or scales and the coherent structure might be easily extracted. In this problem, three types of image structure, namely the large-scale structure near the center of the jet, coherent structure in the shear layer, and the small-scale vortices throughout the entire flow field, which dominate the turbulent structure, were easily extracted. By increasing the Reynolds number, the large-scale structure becomes weaker, and the scales of active vortices and coherent structure decrease.

1. Introduction

Turbulent jets exhibit a complex structure with a wide range of coexisting scales and a variety of shapes in the dynamics. Coherent structures existing in turbulent jets are responsible for most of the momentum transfer. Many identification techniques, such as image processing, spectral analysis, spatial correlation functions, proper orthogonal decomposition, stochastic estimation and pattern recognition, are well established to determine complex structures. Recently, Catrakis and Dimotakis[1] reported two-dimensional spatial measurements of the jet-fluid concentration field. They presented the scale distributions and fractal dimensions measured by level sets of concentration, and showed the shape complexity of irregular surface based on area-volume measurements of images. However, the local scales with respect to space-time change continuously for turbulence, and a complex turbulent structure in terms of space, scale and strength has not yet been clarified. It is well known that the identification of coherent structures requires the acquisition of detailed quantitative data on such structural characteristics as location, size, strength, etc. Until now, traditional analytical techniques could not provide us sufficient or detailed information. Laufer[2] pointed out that the conditional sampling measurement had been hiding very important features of turbulence. To solve these problems, we should develop more powerful identification or analytical techniques. Recently, Li et al.[3-5] applied one-dimensional continuous and discrete wavelet transforms to analyze the experimental velocity signals of a plane turbulent jet in the dimensions of time and frequency. Additionally, Li[6-10] then proposed the wavelet correlation method and wavelet spatial statistics based on wavelets, and revealed the structure of eddy motion and coherent structures in turbulent shear flow in both Fourier and physical spaces. These studies indicated that the wavelet technique offered the potential to extract new information from the turbulent field, however, they are limited to the analysis of turbulent structure based on one-dimensional wavelet transform. To gain deeper insight into multi-scale structures and coherent structures in turbulent flows, it is important to analyze the full field by image processing. Although there have been several studies[11-15] that applied two or three-dimensional wavelet transform to full-field measurements or simulation data, they have thus far been concerned with continuous wavelet transform. In spite of the fact that coefficients of continuous wavelet transform may extract the characterization of local regularity, it is not possible to reconstruct the original function because the mother

*[1] Received December 21st, 1998.
*[2] Department of Mechanical Engineering, Kagoshima University, Kagoshima, Japan.
*[3] Department of Mechanical Engineering, Nihon University, Tokyo, Japan.
*[4] Department of Electrical & Electronic Engineering, Hosei University, Tokyo, Japan.
*[5] Shirayuri Women's College, Tokyo, Japan.

wavelet function is a non-orthogonal function. In turbulent flow image processing, it is of great significance to study the image components of various scales that can reconstruct the original image based on the orthogonal wavelet transform.

One of the dominate principal analytical tools in image processing is Fourier analysis, which can be used to convert point data into a form that is useful for analyzing frequencies. In some problems, however, Fourier analytic techniques are inadequate or lead to extremely onerous computations. One case is that each Fourier coefficient contains complete information about the behavior of images at one scale of frequency but no information about its behavior at other scales or frequencies. In contrast, many applications require the analysis of a series on a broader scale. For example, a region of rapid change in a series can only be detected by examining many points at once. A wavelet is a bandpass filter with additional space location capability. In order to apply the wavelets to the field of image processing, Mallat and Meyer formulated the theory of multiresolution analysis in the fall of 1986, and provided a natural framework for the understanding and construction of wavelet bases. The goal of the multiresolution analysis is to get a representation of a function that is written in a parsimonious manner as a sum of its essential components. That is, a parsimonious representation of a function not only preserves the interesting features of the original function, but also expresses the function in terms of a relatively small set of coefficients. Now, multiresolution analysis is mainly applied to image compression, image editing, multiscale edge detection, and texture discrimination.

The aim of this paper is to apply two-dimensional orthogonal wavelets or multiresolution analysis to the digital imaging photographs of a jet flow in a farfield in order to reveal the multiresolution turbulent structures and to extract the most essential scales governing turbulence.

2. Basic Theory of Two-Dimensional Orthogonal Wavelets

In this section, we introduce the definitions of two-dimensional wavelet transform before applying them to image analysis. Let us consider a two-dimensional scalar field $f(\vec{x})$ and isotropic mother wavelet $\psi(\vec{x})$ by treating $\vec{x}=(x_1, x_2)$ as a vector. The family of wavelet functions $\psi_{\vec{b},a}(\vec{x})$, which is translated by position parameter $\vec{b}\in R^2$ ($\vec{b}=(b_1, b_2)$) and dilated by scale parameter $a\in R^+$, is written as

$$\psi_{\vec{b},a}(\vec{x})=\frac{1}{a}\psi\left(\frac{\vec{x}-\vec{b}}{a}\right), \qquad \ldots.(1)$$

where $\psi(\vec{x})=\psi(|\vec{x}|)$ and $\psi(\vec{x})$ satisfy the admissibility condition

$$C_\psi=\int_{-\infty}^{\infty}\int_{-\infty}^{\infty}\frac{|\hat{\psi}(\vec{\omega})|^2}{|\vec{\omega}|}d^2\vec{\omega}<\infty, \qquad \ldots.(2)$$

i.e., (1) compact support or sufficiently fast decay;

(2) $\int_{-\infty}^{\infty}\int_{-\infty}^{\infty}\psi(\vec{x})d^2\vec{x}=0$.

Several functions, for example, 2-D Morelet wavelet, Halo wavelet and so on, are often used as the mother wavelet in the area of fluid mechanics.

The continuous wavelet transform of $f(\vec{x})$ can be defined as

$$\begin{aligned}Wf(\vec{b}, a)&=\int_{-\infty}^{\infty}\int_{-\infty}^{\infty}f(\vec{x})\psi_{\vec{b},a}(\vec{x})d^2\vec{x}\\&=\frac{1}{a}\int_{-\infty}^{\infty}\int_{-\infty}^{\infty}f(\vec{x})\psi\left(\frac{\vec{x}-\vec{b}}{a}\right)d^2\vec{x}.\end{aligned} \qquad \ldots.(3)$$

The coefficients of continuous wavelet transform $Wf(\vec{b}, a)$ can be interpreted as the relative contribution of scale a to the scalar field $f(\vec{x})$ at position $\vec{b}$.

If the mother wavelet is admissible, the inversion formula can be written as

$$\begin{aligned}f(\vec{x})&=\frac{1}{C_\psi}\int_{-\infty}^{\infty}\int_{-\infty}^{\infty}\int_{0}^{\infty}a^{-3}Wf(\vec{b}, a)\psi_{\vec{b}a}(\vec{x})da d^2\vec{b}\\&=\frac{1}{C_\psi}\int_{-\infty}^{\infty}\int_{-\infty}^{\infty}\int_{0}^{\infty}a^{-4}Wf(\vec{b}, a)\psi\left(\frac{\vec{x}-\vec{b}}{a}\right)da d^2\vec{b}.\end{aligned} \qquad \ldots.(4)$$

The two-dimensional continuous wavelet transform has proved to be useful in many applications[11-15] in the area of fluid mechanics, but it is a non-orthogonal decomposition. Therefore, for actual image analysis, orthogonal or discrete wavelet transform is preferred. In the discrete wavelet transform, the dilation parameter a and translation parameter $\vec{b}$ both take only discrete values in Eq. (3). For a scale a, we choose the integer (positive and negative) powers of one fixed dilation parameter $a_0>1$ (i.e., a_0^m), and different values of m correspond to different widths of wavelets. It follows that the discretization of the translation parameter $\vec{b}$ should depend on m: narrow wavelets (high frequency) are translated by small steps in order to cover the entire field, while wider wavelets (lower frequency) are translated by large steps. Since the width of the wavelets is proportion to a_0^m, we choose therefore to discretize $\vec{b}$ by $\vec{b}=\vec{n}b_0a_0^m$, where b_0 is fixed. Starting from a one-dimensional wavelet basis $\psi_{m,n}(x)=a_0^{-m/2}\psi(a_0^{-m}x-nb_0)$, the two-dimensional wavelet basis simply takes the tensor product functions generated by two one-dimensional bases:

$$\Psi_{m_1,n_1;m_2,n_2}(x_1, x_2)=\psi_{m_1,n_1}(x_1)\psi_{m_2,n_2}(x_2). \qquad \ldots.(5)$$

For some very special choices of $\psi(x)$ and a_0, b_0, the $\psi_{m,n}(x)$ constitutes an orthonormal basis. In particular,

if we choose $a_0=2$, $b_0=1$, then there exists $\psi(x)$, with good physics-frequency localization properties, such that

$$\Psi_{m_1,n_1;m_2,n_2}(x_1, x_2)= 2^{-(m_1+m_2)/2}\psi(2^{-m_1}x_1-n_1)\psi(2^{-m_2}x_2-n_2) \quad \ldots.(6)$$

constitutes a two-dimensional orthogonal basis. In this basis, the two variables x_1 and x_2 are dilated separately. The oldest example of a function $\psi(x)$ for which $\psi_{m,n}(x)$ constitutes an orthogonal basis is the Haar function, constructed long before the term "wavelet" was coined. In the last ten years, various orthogonal wavelet bases have been constructed; for example, Meyer basis, Daubechies basis, Coifman basis, Battle-Lemarie basis, Baylkin basis, spline basis, etc. They provide excellent localization properties in both physical and frequency spaces. In this study, we employ Daubechies basis to analyze the flow image.

The two-dimensional discrete wavelet transform is given by

$$Wf_{m_1,n_1;m_2,n_2}=\int_{-\infty}^{\infty}\int_{-\infty}^{\infty} f(\vec{x})\Psi_{m_1,n_1;m_2,n_2}(\vec{x})d^2\vec{x}. \quad \ldots.(7)$$

The reconstruction of the original scalar field can be achieved by using

$$f(\vec{x})=\sum_{m_1}\sum_{m_2}\sum_{n_1}\sum_{n_2} Wf_{m_1,n_1;m_2,n_2}\Psi_{m_1,n_1;m_2,n_2}(\vec{x}). \quad \ldots.(8)$$

The total energy of the scalar field is given by summing all of the scales and components as follows

$$\sum_{i,j}(f(x_1^i, x_2^j))^2=\sum_{m_1}\sum_{m_2}\sum_{n_1}\sum_{n_2}(Wf_{m_1,n_1;m_2,n_2})^2. \quad \ldots.(9)$$

3. Two-Dimensional Multiresolution Analysis

In mathematics, multiresolution analysis consists of a nested set of linear function spaces V_j with the resolution of functions increasing with j. More precisely, the closed subspaces V_j satisfy

$$\cdots V_2\subset V_1\subset V_0\subset V_{-1}\subset V_{-2}\cdots, \quad \ldots.(10)$$

with

$$\bigcup_{j\in Z} V_j=L^2(\Re^2) \quad \text{and} \quad \bigcap_{j\in Z} V_j=\{o\}. \quad \ldots.(11)$$

The basis functions for the subspaces V_j are called scaling functions of the multiresolution analysis.

For every $j\in Z$, define the wavelet spaces W_j to be the orthogonal complement in V_{j-1} of V_j. We have

$$V_{j-1}=V_j\oplus W_j \quad \ldots.(12)$$

and

$$W_j\perp W_{j'} \quad \text{if} \quad j\neq j', \quad \ldots.(13)$$

(i.e., any function in V_{j-1} can be written as the sum of a unique function in V_j and a unique function in W_j). In $L^2(\Re^2)$, the orthogonal basis for W_j is the family of wavelets $\Psi_{m_1,n_1;m_2,n_2}(x_1, x_2)$ that is defined in Eq. (6). Thus, $L^2(\Re^2)$ can be decomposed into mutually orthogonal subspaces, and can be written as

$$L^2(\Re^2)=\bigoplus_{j\in Z} W_j. \quad \ldots.(14)$$

The details regarding the wavelet transform and multiresolution analysis can be found in many references.[16]

4. Multiresolution Image Analysis of a Turbulent Jet

It is well known that an image often includes too much information for real-time vision processing. The multiresolution algorithm processes less image data by selecting the relevant details that are necessary to perform a particular recognition task.

In order to gain deeper insight into the multi-scale structures and coherent structures, we apply multiresolution analysis to the digital-imaging photographs of a turbulent jet that were experimentally obtained by Catrakis and Dimotakis.[1] The original image is decomposed into the wavelet spaces.

The experiment was carried out on liquid-phase turbulent-jet flows, and images of slices that relied on laser-induced fluorescence digital-imaging techniques were obtained. Transverse sections in the far field of the jet flow, at downstream position z $d=275$ (jet-nozzle diameter d is 2.54 mm), were recorded on a cryogenically cooled 1024×1024 pixel CCD camera. The field of view spans $l_0\cong42$ cm, resulting in a pixel resolution of $\lambda_p\cong420\,\mu$m. More details are given in Catrakis and Dimotakis.[1]

In this paper, black-and-white images of jet flow slices are expressed in a numerical form as a function $f(x_1, x_2)$ over two dimensions in which the function value $f(x_1^0, x_2^0)$ represents the "gray scale" value of the image at the position or pixel values (x_1, x_2). The "gray scale" values are then normalized to one.

The procedure of this multiresolution analysis can be summarized in two steps:

(1) Wavelet coefficients or the wavelet spectrum of an image is computed based on the discrete wavelet transform of Eq. (7).

(2) The inverse wavelet transform of Eq. (8) is applied to wavelet coefficients at each wavelet level, and image components are obtained at each level or scale or in the wavelet spaces.

It is evident that the sum of all image components in the wavelet spaces can reconstruct the original image. As described above, there are several families of orthonormal wavelet basis that construct the wavelet spaces. In this paper, we use the Daubechies family[16] with an index of $N=20$, which is not only orthonormal but also has smoothness and compact support.

At first, the original image of the jet-fluid concentration with $Re \cong 4.5 \times 10^3$ at downstream position $z/d = 275$, as shown in Fig.1, is computed by the two-dimensional orthogonal wavelet transform. The result of its wavelet coefficients normalized to one is shown in Fig. 2. Back and white pixels correspond respectively to smaller and larger wavelet coefficients. It is evident that the larger wavelet coefficients concentrate on the range of smaller numbers of wavelet coefficient (i.e., in the large-scale range). This feature shows that large-scale motion is active and contains turbulent energy. If wavelet image compression is used, we may obtain a higher compressed turbulent image that only contains information on the most essential scales governing turbulence.

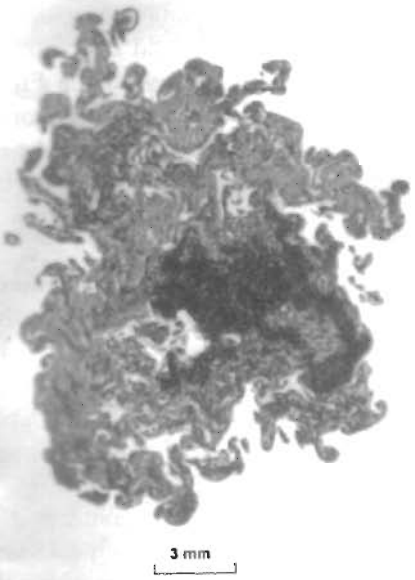

Fig. 1. Original image of a turbulent jet at $Re \cong 4.5 \times 10^3$.

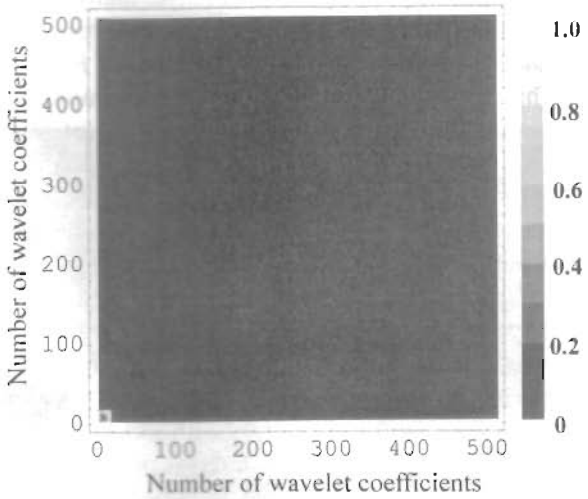

Fig. 2. Wavelet coefficients of image in a turbulent jet at $Re \cong 4.5 \times 10^3$.

Then, the original image is decomposed into six wavelet spaces based on the inverse wavelet transform. The scale of wavelet space is usually called the level, and levels 1 to 6 represent large- to small-scale in this study. The image components with six levels are displayed in Fig. 3. The sum of six image components can completely reconstruct the original image. In order to investigate the frequency character of six wavelet spaces, image components of six levels are respectively analyzed by two-dimensional Fourier Transform. In this study, the relationships between level and scale when using the Daubechies family with index $N = 20$ are listed in Table 1.

In Fig. 3, false colors have been assigned to the scalar values of image components; the highest concentration is displayed as deep red and the lowest as purple. These images provide information on the multi-scale structures in turbulent jet flow and the important scales that dominate the flow structure may be easily extracted. In the image component (Fig. 3a) of level 1, which corresponds to the broader scale of $a = 43.0$–107.5 mm, the blue boundary of the large-scale flow region may be clearly seen. A large peak that contains three peaks can be clearly observed near the center of the jet flow. By comparing the original image, these peaks imply that a large-scale structure consists of three vortices. They are the uppermost and energy-containing vortices. With the broader scale of $a = 14.3$–43.0 mm, as shown in the image of level 2 (Fig. 3b), a lot of stronger peaks mainly appear in the edge of the flow region, and correspond to the positions of vortices at this scale range. These vortices are more active in the shear layer and dominate the turbulent mixing process, which are referred to as the coherent structure of the problem. As the scale decreases to $a = 7.2$–14.3 mm at level 3 in Fig. 3c, peaks mainly concentrate on islands or lakes (as described in Catrakis and Dimotakis[1]) of the flow region edge. The distribution of peaks indicates that vortices also undertake the turbulent mixing process within this scale range in this region. When broader scaling reaches to $a = 3.6$–7.2 mm, as shown in the image of level 4 (Fig. 3d), edges of the vortex within this scale range can be clearly observed. As resolution increases to $a = 1.8$–3.6 mm, a finer approximation of the original image can be obtained at level 5 (Fig. 3e). A clear distribution of vortex edges with smaller-scale can be observed, which is the "zoom-in" the image of level 4. This is an important

Table 1. The relationship between level and scale for Daubechies bases with index $N = 20$.

	Level 1	Level 2	Level 3	Level 4	Level 5	Level 6
Scale (mm)	43.0–107.5	14.3–43.0	7.2–14.3	3.6–7.2	1.8–3.6	0.8–1.8

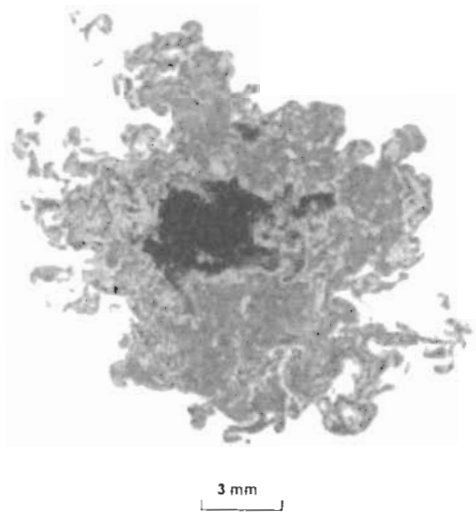

Fig. 5. Original image of a turbulent jet at $Re \cong 9.0 \times 10^3$.

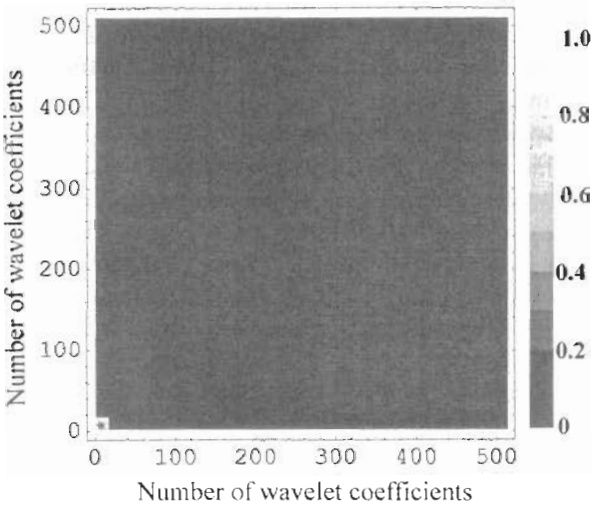

Fig. 6. Wavelet coefficients of image in a turbulent jet at $Re \cong 9.0 \times 10^3$.

feature of multiresolution analysis. The image of level 6 (Fig. 3f) describes the finest turbulent structure of the original image with a broader scale of $a = 0.8$–1.8mm. The smallest-scale vortex in this problem can be observed everywhere in the interior of the flow. This means that the smallest-scale vortices exist throughout the entire flow field. From the above results, it can be said that the edgesof the vortices at different resolutions or scales and the coherent structure may be easily extracted by wavelet multiresolution analysis.

To sum up the major characteristics of flow structures, three types of flow structure, the large-scale structure near the center of the jet flow, the coherent structure in the shear layer and the small-scale vortices throughout the entire flow field, are of most significance and dominate the turbulent structure in the jet flow.

In order to gain deeper insight into the dominant structures, the following computation is performed. The sum of level 1 and level 2 produces the image in Fig. 4 (a), the sum of level 3 and level 4 produces the image in Fig. 4(b) and the sum of level 5 and level 6 produces the image in Fig. 4(c). Figure 4 describes a turbulent structure within three important broader scales; that is, the energy-containing structure within large broader scale of $a = 14.3$–107.5 mm, the coherent structure and dominating turbulent mixing process in the shear layer within the medium broader scale of $a = 3.6$–14.3 mm, and the smaller-scale structure within small broader scale of $a = 0.8$–3.6 mm.

By increasing the Reynolds number to $Re \cong 9.0 \times 10^3$, the original image of the jet-fluid concentration at the same downstream position, as shown in Fig. 5, is also analyzed by the two-dimensional orthogonal wavelet transform, and the distribution of its wavelet coefficients is plotted in Fig. 6. Similar to $Re = 4.5 \times 10^3$, the wavelet coefficients exhibit higher magnitude within the large-scale range.

Figure 7 shows the images of multiresolution structures of a turbulent jet flow slice, which are obtained by decomposing the original image (in Fig. 5) into image components of six levels or scales using wavelet multiresolution analysis. Only one peak can be observed near the center of the jet flow within the broader scale of $a = 43.0$–107.5 mm (at level 1) in Fig. 7a. This peak magnifies a large-scale, energy-containing structure. Compared to Fig. 3b, the number of peaks that appears in the edge of the flow region decreases within the broader scale of $a = 14.3$–43.0 mm (at level 2) in Fig. 7b. This means that the large-scale motion becomes weaker as the Reynolds number increases. However, in the scale range of $a = 7.2$–14.3 mm, at levels 3 in Fig. 7c, many stronger peaks can be observed in the edge of the flow region, and the scalar-concentration is higher than that of $Re = 4.5 \times 10^3$. This implies that vortex motions become more active in the shear layer and dominate the turbulent mixing process. It is appropriate to say that the coherent structures appear in this broader scale. When considering the image of level 4 in Fig. 7d, edges of vortices and positions of vortices within the scale range of $a = 3.6$–7.2 mm can be clearly observed, which zoom in the image structure of Fig. 7c (at level 3). As resolution increases to level 5 (Fig. 7e), a finer resolution of the original image can be obtained within $a = 1.8$–3.6 mm. A clear distribution of vortex edges with smaller scale can be observed everywhere in the interior of the flow. The image of level 6 (Fig. 7f) shows the finest structures of light. It is obvious that the smaller-scale motion within the broader scale of $a = 0.8$–1.8 mm becomes weaker.

Using the same method as above, six multiresolution images can be summarized into three image components within three important broader scales in Fig. 8. This figure clearly provides visualization on the energy-containing structure, the coherent structure and the smaller-scale structure within the broader scales of 14.3–

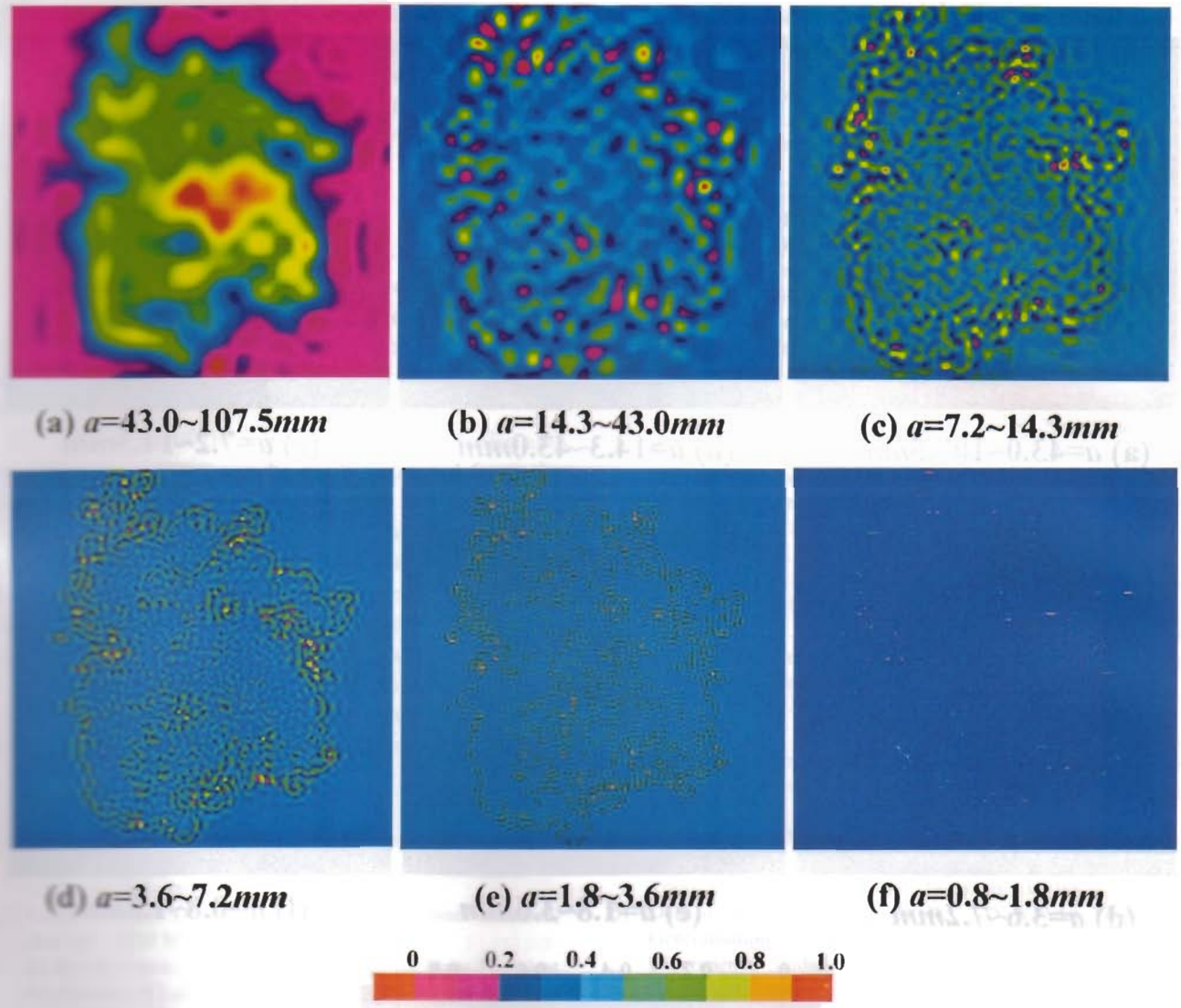

Fig. 3. Multiresolution images of a turbulent jet at $Re \cong 4.5 \times 10^3$.

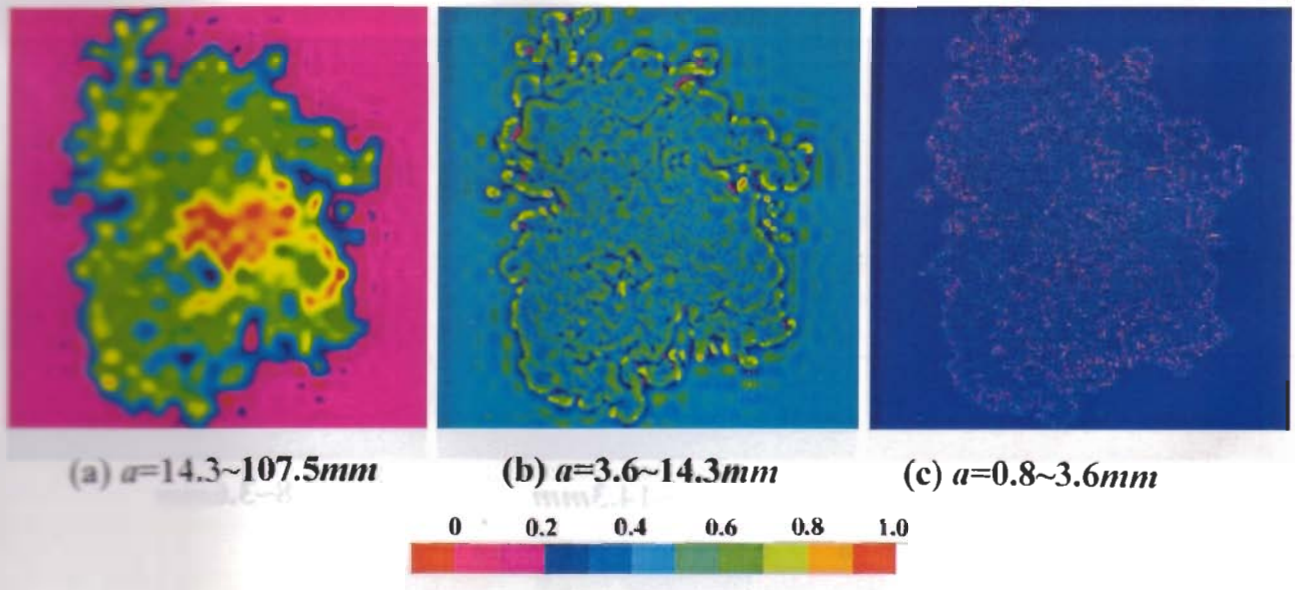

Fig. 4. Sum of multiresolution images in a turbulent jet at $Re \cong 4.5 \times 10^3$.

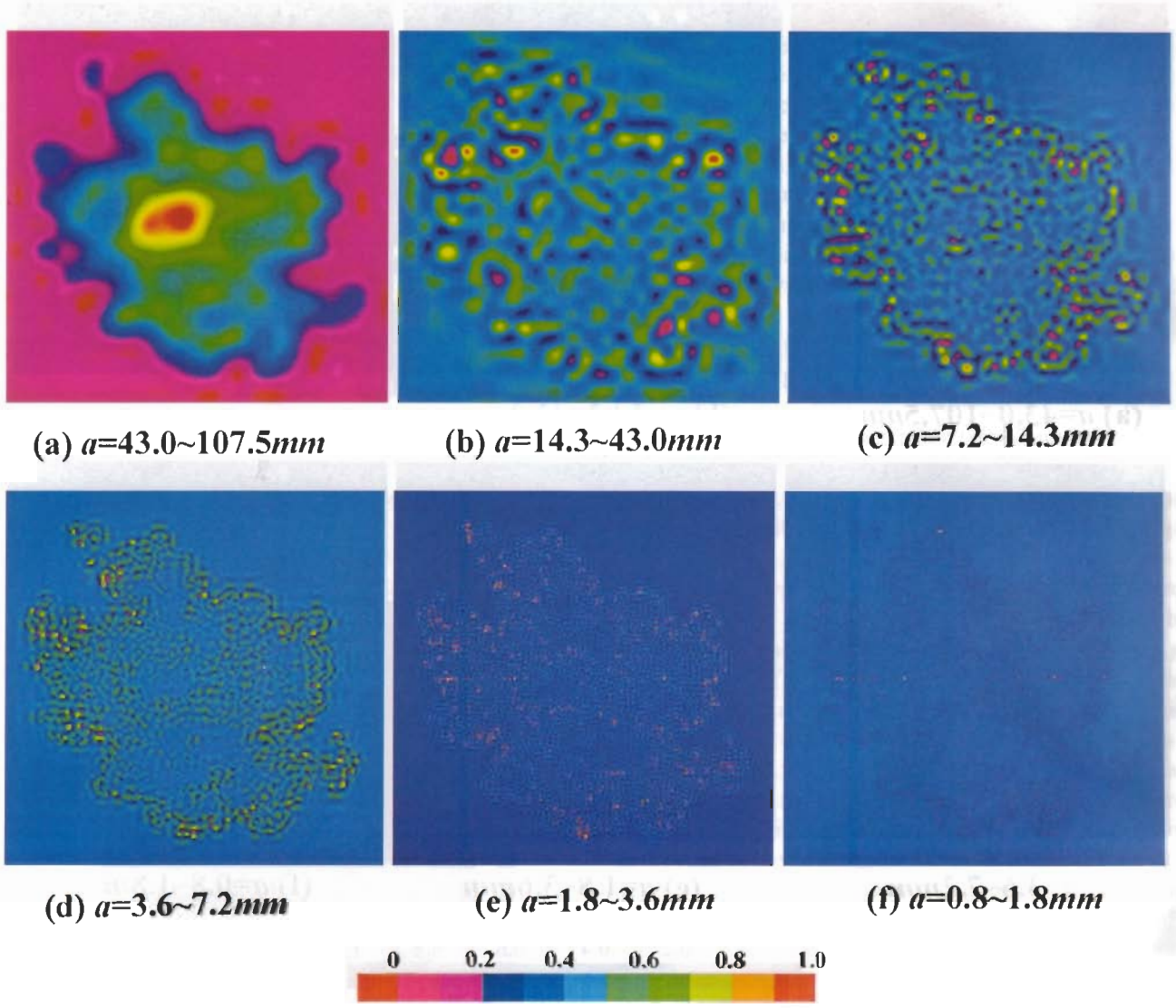

Fig. 7. Multiresolution images of a turbulent jet at $Re \cong 9.0 \times 10^3$.

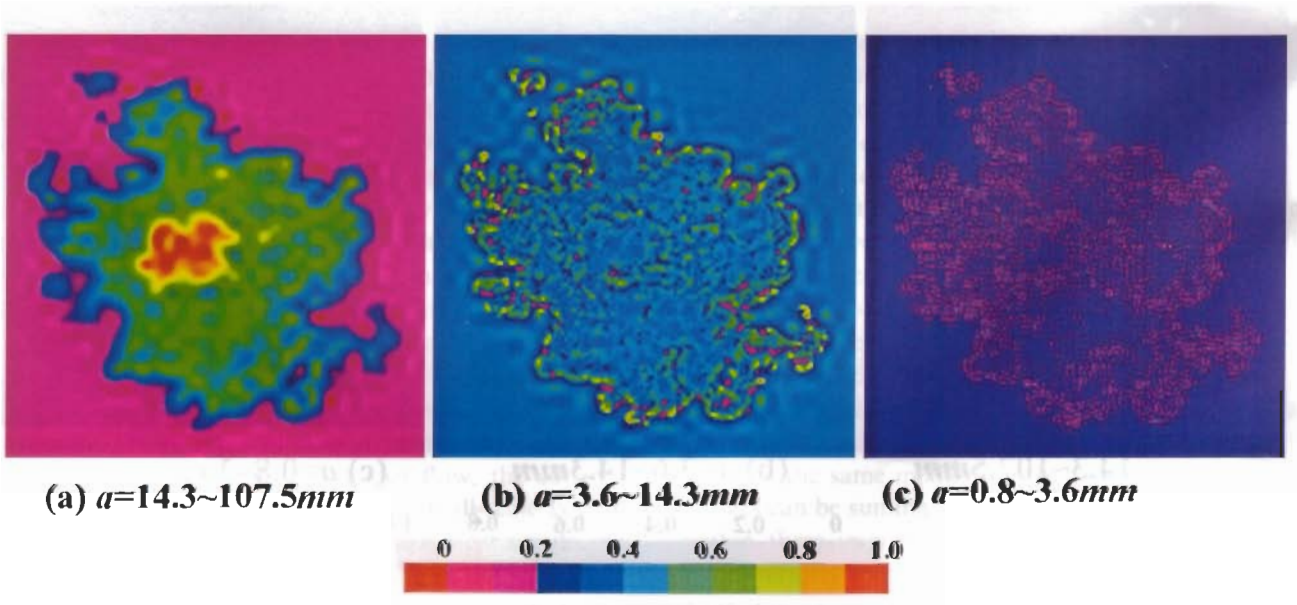

Fig. 8. Sum of multiresolution images in a turbulent jet at $Re \cong 9.0 \times 10^3$.

107.5, 3.6–14.3, and 0.8–3.6 mm, respectively. Compared with Fig. 4, Fig. 8 exhibits that the scalar concentration within medium and small broader scales becomes higher with increases in Reynolds number. It is evident that medium and small vortices are more active and dominate the flow structure at $Re \cong 9.0 \times 10^3$.

5. Concluding Remarks

The major conclusions are summarized as follows:

(1) The image components of different scales can be obtained using two-dimensional orthogonal wavelets, and provide information of the multi-scale structures in jet flows.

(2) The edges of the vortices at different scales and the coherent structure can be easily extracted from the multiresolution images.

(3) Three types of image structures, namely large-scale or energy-containing structure near the center of the jet flow, coherent structure in the shear layer and the small-scale vortices throughout the entire flow field, dominate the turbulent structure in jet slices.

(4) When the Reynolds number is increased, the large-scale motion becomes weaker, and the scales of active vortices and coherent structure decrease.

References

1) Catrakis, H. J. and Dimotakis, P. E.: Mixing in Turbulent Jets: Scalar Measures and Isosurface Geometry, *J. Fluid Mech.*, **317** (1996), pp. 369–406.
2) Laufer, J.: New Trends in Experimental Turbulence Research, *Ann. Rev. Fluid Mech.*, **7** (1975), pp. 307–320.
3) Li, H. and Nozaki, T.: Wavelet Analysis for the Plane Turbulent Jet (Analysis of Large Eddy Structure), *JSME Int. J., Fluids and Thermal Eng.*, **38**, 4 (1995), pp. 525–531.
4) Li, H., Takei, M., Ochi, M., Saito, Y. and Horii, K.: Velocity Correlation Analysis in the Near-Field of a Turbulent Jet with Help of Discrete Wavelet Transform, *ASME FEDSM98-4823* (1998), pp. 1–6.
5) Li, H., Takei, M., Ochi, M., Saito, Y. and Horii, K.: Structure Evaluation of Unsteady Turbulent Flow with Continuous and Discrete Wavelet Transforms, *ASME FEDSM99-7167* (1999), pp. 1–6.
6) Li, H. and Nozaki, T.: Application of Wavelet Cross-Correlation Analysis to a Turbulent Plane Jet, *JSME Int. J., Fluids and Thermal Eng.*, **40**, 1 (1997), pp. 58–66.
7) Li, H.: Wavelet Auto-Correlation Analysis Applied to Eddy Structure Identification of Free Turbulent Shear Flow, *JSME Int. J., Fluids and Thermal Eng.*, **40**, 4 (1997), pp. 567–576.
8) Li, H.: Identification of Coherent Structure in Turbulent Shear Flow with Wavelet Correlation Analysis, *ASME J. Fluids Eng.*, **120**, 4 (1998), pp. 778–785.
9) Li, H.: Wavelet Statistical Analysis of the Near-Field Flow Structure in a Turbulent Jet, *Trans. Japan Soc. Aero. Space Sci.*, **41**, 133 (1998), pp. 132–139.
10) Li, H. and Nozaki, T., Tabata, T. and Oshige, S.: Wavelet Analysis of the Near-Field Structure in a Bounded Jet, *Trans. Japan Soc. Aero. Space Sci.*, **42**, 135 (1999), pp. 27–33.
11) Everson, R. and Sirovich, L.: Wavelet Analysis of the Turbulent Jet, *Phys. Lett.*, **145**, 6 (1990), pp. 314–322.
12) Brasseur, J. G. and Wang, Q.: Structural Evolution of Intermittency and Anisotropy at Different Scales Analyzed Using Three-Dimensional Wavelet Transforms, *Phys. Fluids A*, **4**, 11 (1992), pp. 2538–2554.
13) Spedding, G. R., Browand, F. K., Huang, N. E. and Long, S. R.: A 2-D Complex Wavelet Analysis of an Unsteady Wind-Generated Surface Wave Field, *Dyn. Atmos. Oceans*, **20** (1993), pp. 55–77.
14) Dallard, T. and Browand, F. K.: Scale Transitions at Defect Sites in the Mixing Layer: Application of the 2-D Arc Wavelet Transform, *J. Fluid Mech.*, **247** (1993), pp. 339–368.
15) Dallard, T. and Spedding, G. R.: 2-D Wavelet Transform: Generalisation of the Hardy Space and Application to Experimental Studies, *Eur. J. Mech. B/Fluids*, **12** (1993), pp. 107–134.
16) Daubechies, I.: *Ten Lectures on Wavelets*, Society for Industrial and Applied Mathematics, 1992.